Published in final edited form as:
J Mater Chem. 2012 January 1; 22(35): 18139–18144. doi:10.1039/C2JM32299D.

Zr- and Hf-based nanoscale metal-organic frameworks as contrast agents for computed tomography

Kathryn E. deKrafft[a], **William S. Boyle**[a], **Laurel M. Burk**[b], **Otto Z. Zhou**[b], and **Wenbin Lin**[a]

Wenbin Lin: wlin@unc.edu

[a]Department of Chemistry, CB 3290, University of North Carolina, Chapel Hill, NC 27599 (USA). Fax: 919-962-2388; Tel: 919-962-6320

[b]Department of Physics and Astronomy, University of North Carolina, Chapel Hill, NC 27599 (USA). Tel: 919-962-3297

Abstract

Nanoscale metal-organic frameworks (NMOFs) of the UiO-66 structure containing high Zr (37 wt %) and Hf (57 wt%) content were synthesized and characterized, and their potential as contrast agents for X-ray computed tomography (CT) imaging was evaluated. Hf-NMOFs of different sizes were coated with silica and poly(ethylene glycol) (PEG) to enhance biocompatibility, and were used for in vivo CT imaging of mice, showing increased attenuation in the liver and spleen.

Introduction

X-ray computed tomography (CT) is a widely used biomedical imaging technique that is capable of providing three-dimensional images with excellent spatial resolution.[1, 2] It is an important tool for diagnosing and monitoring diseases and abnormalities throughout the body.[3] CT is based on differences in X-ray attenuation, and a contrast agent is often used to enhance the contrast between the tissue of interest and its surroundings.[3–6] Materials with high electron density have high X-ray attenuation, therefore elements with high atomic numbers (high-Z elements), like iodine, gold, bismuth, and gadolinium, have been considered for use as contrast agents. However, the only CT contrast agents currently approved for clinical use are iodinated aromatic molecules for vascular and organ imaging and barium sulfate for gastrointestinal tract imaging. The utility of CT imaging with small-molecule contrast agents is limited by their nonspecific distribution, rapid renal clearance, and fast extravasation from blood and lymphatic vessels.[3–6] As a consequence, large doses of small molecule contrast agents (typically 30 g of I or 70 g total material) must be administered to achieve adequate contrast, sometimes causing adverse reactions for the patients.[3, 5]

Many of the limitations of molecular contrast agents can be overcome by nanoparticulate contrast agents that can carry a high payload and be functionalized to increase blood circulation times and to endow target specificity.[7] Nanoparticles do not readily diffuse into extravascular space or undergo rapid renal clearance, thus allowing adequate time for accumulation at a disease site. Several nanoparticle systems including Bi_2S_3,[8] gold,[9, 10] and iodinated organic nanoparticles,[11–13] have recently been evaluated as next-generation CT contrast agents. However, it is still challenging to formulate nanoparticles with high

Correspondence to: Wenbin Lin, wlin@unc.edu.

†Electronic Supplementary Information (ESI) available: characterization of **Hf-UiO**, **Hf-UiO**@SiO_2, **Hf-UiO**@SiO_2@PEG, and **Hf-NMOF**@SiO_2@PEG. CT images of **Hf-NMOF**@SiO_2@PEG. See DOI: 10.1039/b000000x/

loadings of high-Z elements that are also nontoxic and able to be cleared from the body in a timely fashion. We previously reported nanoparticles of one-dimensional iodinated coordination polymers as potential CT contrast agents.[14] While these iodinated coordination polymer nanoparticles had several advantages over molecular contrast agents and other types of nanoparticles, they did not possess adequate stability to be further functionalized and used *in vivo*. Metal-organic frameworks (MOFs) are crystalline three-dimensional coordination polymers composed of organic bridging ligands that are coordinatively bonded to metal ions or metal ion clusters.[15–18] The synthesis and development of a new class of nanomaterials has recently been demonstrated by scaling down MOFs to the nanoregime.[19, 20] These nanoscale MOFs (NMOFs) have already shown great potential in biosensing,[21] magnetic resonance imaging,[22, 23] and drug delivery.[24]

In this work, NMOFs containing high-Z elements are synthesized and their potential as CT contrast agents is evaluated. Instead of incorporating the high-Z element into the bridging ligand of the structure as in our earlier work,[14] the high-Z elements (hafnium and zirconium) are incorporated into NMOFs in the $M_6(\mu_3\text{-}O_4)(\mu_3\text{-}OH)_4(RCO_2)_{12}$ (M = Zr or Hf) secondary building units. While clinically-used contrast agents are iodinated molecules, iodine is not the best choice for a contrast agent in terms of X-ray attenuation efficiency, but is used mainly due its low toxicity and low cost.[6] Elements with higher attenuation at relevant X-ray photon energies could provide adequate contrast at a lower dose and decrease the amount of radiation to which a patient must be exposed.

UiO-66 is a MOF composed of the Zr-carboxylate cluster $Zr_6(\mu_3\text{-}O_4)(\mu_3\text{-}OH)_4(RCO_2)_{12}$, which serves as a secondary building unit, bridged by benzenedicarboxylate linkers.[25] UiO-66 is more chemically, thermally, and mechanically stable compared to other MOFs, owing mainly to the strength of the Zr-carboxylate bond.[26] While Zr has an atomic number of 40, which may make it useful as a component of a CT contrast agent, Hf shows similar chemical behaviors and has an even higher atomic number (72). Therefore, a Hf analog of the Zr UiO-66 MOF has been made for the first time, and has been evaluated as a CT contrast agent in vivo.

Experimental

Materials and methods

All starting materials were purchased from Fisher or Aldrich and used without further purification. Proton nuclear magnetic resonance spectroscopy (^{1}H NMR) spectra were recorded on a Bruker NMR 400 at 400 MHz and referenced to the proton resonance resulting from incomplete deuteration of deuterated dimethyl sulfoxide (DMSO-d_6, δ 2.50). Thermogravimetric analysis (TGA) was performed using a Shimadzu TGA-50 equipped with a platinum pan, and all samples were air-dried and heated at a rate of 4 °C per minute under air. Scanning electron microscopy (SEM) was used to image the particles, using a Hitachi 4700 field emission scanning electron microscope. A Cressington 108 Auto Sputter Coater equipped with a Au/Pd (80/20) target and an MTM-10 thickness monitor was used to coat the samples with a conductive layer before taking SEM images. Each SEM sample was prepared by first suspending the nanomaterial in ethanol, then a drop of the suspension was placed on a glass slide and the solvent was allowed to evaporate. Transmission electron microscopy (TEM) was obtained on a JEOL 100CX-II Transmission Electron Microscope using carbon-coated copper grids to hold samples. Size and zeta potential information was obtained on a Malvern ZetaSizer dynamic light scattering instrument. Infrared spectroscopy (IR) was performed using a Bruker Alpha-T Fourier Transform Infrared Spectrometer in attenuated total reflectance (ATR) mode. Powder X-ray diffraction (PXRD) analyses were carried out using a Bruker SMART Apex II diffractometer using Cu radiation. The PXRD patterns were processed with the Apex II package using the phase ID plugin.

CT phantom and *in vivo* images and X-ray attenuation data were obtained using a micro-computed tomography scanner equipped with a carbon nanotube based field emission micro-focus X-ray source. All CT scans were done at 50 kVp, 0.7 mA, 0.5 mm Al filtration, and 50 msec exposure per projection. Four hundred projections were used over a circular orbit of 200° at a step angle of 0.5° and were reconstructed at 76 μm isotropic voxel spacing. In vivo imaging was carried out using protocol approved by University of North Carolina Institutional Animal Care and Use Committee. The animals were anesthetized with 1–2% isoflurane at a flow rate of 1.5–2 L min^{-1} from a vaporizer. The anesthetized animals were placed over the pressure sensor in the mouse sample holder and secured with adhesive restraints. The animals were put in the prone position such that the respiration sensor was approximately in the position of the abdomen to achieve maximum sensor coupling. To obtain the cardiac signals, ECG electrodes were taped to the footpads. With the camera running at 1 frame per second, the scan time was typically 15–20 min depending on the mouse respiration and heart rates.

Synthesis of PEG and nanoscale metal-organic frameworks

Synthesis of triethoxysilylpropyl carbamoyl-poly(ethylene glycol)2000 ($(OEt)_3Si\text{-}PEG_{2000}\text{-}OCH_3$): 1.00 g (0.50 mmol) of poly(ethylene glycol)-2000 monomethylether was dried under vacuum at 100 °C for 5 h. After cooling the PEG to room temperature, it was dissolved in 4 mL anhydrous dimethyl sulfoxide (DMSO). 0.124 mL (0.50 mmol) of distilled (3-isocyanatopropyl)triethoxysilane was then added, followed by 1 μL (0.742 mg, 5.7 μmol) of diisopropylethylamine (Hünig's base). The reaction was stirred at room temperature under N_2 for 12 h. The DMSO was removed under vacuum at 60 °C. ^{1}H NMR (DMSO-d_6, 400 MHz): 0.51 (t, 2H), 1.14 (t, 9H), 1.43 (t, 2H), 2.92 (q, 2H), 3.35 (s, 3H), 3.50 (s, 174H), 3.73 (q, 6H), 4.03 (t, 2H), 7.22 (t, 1H).

Synthesis of **Zr-UiO: Zr-UiO** was synthesized using a reported procedure.[25] 1,4-benzene dicarboxylic acid (37.7 mg, 0.23 mmol) and $ZrCl_4$ (52.9 mg, 0.23 mmol) were dissolved in 26.4 mL DMF. This solution was sealed in a Teflon-lined autoclave and heated in an oven at 120 °C for 24 h. After cooling to room temperature, the resulting solid was isolated be centrifugation at 10,000 rpm for 10 min. After removing the supernatant, the solid was washed three times, once using 20 mL of DMF, then twice using 10 mL of ethanol each time. For each wash, the particles were redispersed by sonication and then recovered by centrifugation at 10,000 rpm for 10 min. Yield: 48.8 mg (76.9%)

Synthesis of **Hf-UiO**: 1,4-Benzene dicarboxylic acid (45.1 mg, 0.27 mmol) and $HfCl_4$ (87.1 mg, 0.27 mmol) were dissolved in 26.4 mL of DMF, and acetic acid (13.2 μL, 0.23 mmol) was added. This solution was sealed in a Teflon-lined autoclave and heated in an oven at 100 °C for 48 h. After cooling to room temperature, the resulting solid was isolated and washed as described for **Zr-UiO**. Yield: 77.6 mg (78.2%)

Synthesis of **Hf-UiO**@SiO_2: **Hf-UiO** (60.0 mg) was dispersed in 10 mL of ethanol. This dispersion was added to a solution of 2.0 mL ammonium hydroxide (14.8 M, 30.0 mmol) in 138 mL of ethanol, then TEOS (18.0 μL, 81.2 μmol) was added. The final 150-mL reaction mixture contained 0.4 mg of particles/mL with 0.2 M NH_4OH and 0.406 mM TEOS. The reaction was stirred at room temperature for 2 h, then the resulting particles were isolated by centrifugation and washed with ethanol, as described for **Zr-UiO**. Yield: 52.8 mg (76.4%)

Synthesis of **Hf-UiO**@SiO_2@PEG: **Hf-UiO**@SiO_2 (45.0 mg) was dispersed in a 10-mL solution of $(OEt)_3Si\text{-}PEG_{2000}\text{-}OCH_3$ (15.0 mg, 6.8 μmol) in ethanol. This dispersion was added to a solution of 0.305 mL ammonium hydroxide (14.8 M, 4.5 mmol) in 4.7 mL of ethanol. The final 15-mL reaction mixture contained 3 mg of particles/mL with 0.3 M NH_4OH and 0.45 mM PEG. The reaction was stirred at room temperature for 21 h, then the

resulting particles were isolated by centrifugation and washed with H_2O and methanol, as described for **Zr-UiO**. Yield: 40.5 mg (71.8%)

Synthesis of **Hf-NMOF**: 1,4-Benzene dicarboxylic acid (21.9 mg, 0.13 mmol) and $HfCl_4$ (42.3 mg, 0.13 mmol) were dissolved in 26.4 mL of DMF. This solution was sealed in a Teflon-lined autoclave and heated in an oven at 100 °C for 48 h. After cooling to room temperature, the resulting solid was isolated and washed as described for **Zr-UiO**. Yield: 41.6 mg (86.4%)

Synthesis of **Hf-NMOF**@SiO_2: **Hf-NMOF** (60.0 mg) was dispersed in 10 mL of ethanol. This dispersion was added to a solution of 1.52 mL ammonium hydroxide (14.8 M, 22.5 mmol) in 138.47 mL of ethanol, then TEOS (9.0 μL, 40.6 μmol) was added. The final 150-mL reaction mixture contained 0.4 mg of particles/mL with 0.15 M NH_4OH and 0.20 mM TEOS. The reaction was stirred at room temperature for 1 h, then the resulting particles were isolated by centrifugation and washed with ethanol, as described for **Zr-UiO**. Yield: 56.4 mg (94.0%)

Synthesis of **Hf-NMOF**@SiO_2@PEG: The same procedure as for **Hf-UiO**@SiO_2@PEG was used, except **Hf-NMOF**@SiO_2 was used instead of **Hf-UiO**@SiO_2. Yield: 45.0 mg (100%).

Results and discussion

Synthesis and characterization of Zr- and Hf-UiO

Nanoparticles of the UiO-66 MOF with the formula $Zr_6O_6(OH)_4(BDC)$ (**Zr-UiO,** BDC = 1,4-benzenedicarboxylate) were synthesized by the reported solvothermal method.[25] Equal molar amounts of $ZrCl_4$ and benzene dicarboxylic acid (H_2BDC) were dissolved in N,N′-dimethylformamide (DMF) and heated at 120 °C in a sealed vessel for 24 h. The resulting particles were observed by scanning electron microscopy (SEM) and transmission electron microscopy (TEM) to be ~50 nm cubes, many intergrown to form clusters up to ~200 nm in size (Fig. 1A, S1A). The reported crystal structure of UiO-66 was solved using powder X-ray diffraction (PXRD) data.[25] **Zr-UiO** was shown to match the UiO-66 structure by PXRD (Fig. 1C). The peak at 12°, which does not appear in the simulated pattern, is due to solvent molecules within the pores of the as-synthesized MOF, as it disappears when the MOF is desolvated.[25]

The Hf analog of **Zr-UiO** was also synthesized by a solvothermal method, but using the same conditions as for **Zr-UiO** resulted in poorly crystalline particles intergrown into clusters as large as 3 μm, with a large size distribution. In order to obtain more monodisperse smaller particle clusters with better crystallinity, small amounts of acetic acid were added as a modulator. **Hf-UiO** ($Hf_6O_6(OH)_4(BDC)$) was synthesized by heating a solution of equal molar $HfCl_4$ and H_2BDC with 0.85 equivalents of acetic acid in DMF at 100 °C in a sealed vessel for 48 h. Addition of terminating ligands has recently been introduced as a method to control NMOF growth.[27–29] Acetic acid competes with BDC for coordination with the metal cations of **Hf-UiO** and presumably also modulates growth by binding with soluble Hf^{4+} species in solution. The resulting particles were observed by SEM and TEM to be 50–200 nm clusters of intergrown ~30 nm cubes (Fig. 1B, S1B). The PXRD pattern of **Hf-UiO** is very similar to that of **Zr-UiO**, indicating their isostructural nature (Fig. 1C). Thermogravimetric analysis (TGA) of **Zr-UiO** and **Hf-UiO** shows 50.2% and 32.4% weight loss, respectively, due to dehydroxylation from 250–300 °C and decomposition of BDC from 420–520 °C to leave behind ZrO_2 and HfO_2 (Fig. 1D). The expected weight losses calculated from the formulas are 55.6% and 43.3% for **Zr-UiO** and

Hf-UiO, respectively. The lower weight losses observed could be due to some amorphous Zr/Hf oxides formed during synthesis and trapped in the pores of the NMOF.

Phantom CT studies

Phantom studies were conducted with **Hf-UiO** and **Zr-UiO** to evaluate their X-ray attenuation properties. Aqueous dispersions of each type of NMOF underwent CT scans with concentrations ranging from 0.0–.20 M Hf or Zr. For comparison, various concentrations of Iodixanol, a clinically used iodinated contrast agent, were also scanned. **Hf-UiO** contains 57.3 wt% Hf and **Zr-UiO** contains 37.0 wt% Zr, while Iodixanol contains 49 wt% I. The Hounsfield unit (HU)[30] value is an indicator of the ability of a material to attenuate X-rays with respect to water (0 HU). For images taken at 50 kVp (peak voltage), the slopes of the lines produced by plotting HU values against Hf/Zr/I concentrations for **Hf-UiO**, **Zr-UiO**, and Iodixanol are 10740±390, 5600±180, and 5390±230 HU/M, respectively (Fig. 2). These values are consistent with the relative attenuation coefficients of Hf, Zr, and I at the relevant photon energies, shown in Fig. 2E on a per mol basis, derived from data reported by NIST (see Supporting Information, Fig. S2).[31] The X-ray source produces photons with a wide energy distribution, with the kVp beingthe maximum, and the lowest energy photons are removed by filtration.[32] In this case, with a kVp of 50 keV, the photon energy distribution is centered around 22 keV.

Attenuation coefficients increase sharply at the K shell electron binding energy (K edge) of a particular element. K edge energy is higher for heavier elements, and the K edge energies for Zr, I, and Hf, are 18.0, 33.2, and 65.4 keV, respectively. While Zr has higher attenuation than I in the 18.0–33.2 eV range, the higher attenuation of I below and above this range makes the overall attenuation of Zr and I very similar on a per mol basis. Hf has higher attenuation than both Zr and I by about a factor of two. The enhancement in attenuation compared to these lighter elements would be even more pronounced at the higher kVp values (typically 120 kVp) used clinically for imaging human patients, due to the higher energy of the K edge. A Hf-based CT contrast agent could provide superior contrast at a lower dose compared to an I-based agent, and could decrease the amount of radiation to which the patient must be exposed.

Functionalization of Hf-UiO nanoparticles

Based on the encouraging results from phantom studies, we decided to evaluate the potential of **Hf-UiO** as a CT contrast agent in vivo. Our previous studies showed that most NMOFs are not stable under physiological conditions due to the presence of many competing binding ligands such as phosphate and carbonate ions.[33, 34] Indeed it was found that phosphate in phosphate buffered saline (PBS) can compete with carboxylate groups in **Hf-UiO** to form $Hf(PO_4)_x$. We have also shown that some of the NMOFs could be coated with an amorphous shell of silica to slow down the NMOF decomposition so that the imaging or therapeutic cargoes will not be prematurely lost.[21, 24, 34] The silica coating can also facilitate attachment of siloxy-derived molecules to increase the biocompatibility of the NMOF particles.[24, 34] Tetraethyl orthosilicate (TEOS) was added to a dispersion of **Hf-UiO** in ethanol with ammonium hydroxide to catalyze hydrolysis and condensation of TEOS to coat the particles with a layer of amorphous silica (**Hf-UiO**@SiO_2). **Hf-UiO**@SiO_2 looks similar to the bare particles by TEM (Fig. 3A), but the presence of silica is indicated by the appearance of a Si-O band in the IR spectrum at 1051 cm^{-1} (Fig. S4). TGA shows an increase in weight remaining corresponding to 13.2 wt% SiO_2 (Fig. 3C). The zeta potential becomes more negative, from −24.6 mV for the bare particles to −32.8 mV for the silica-coated particles, due to deprotonated surface silanol groups.

When nanoparticles are used in vivo, they must be modified with passivating moieties to enhance biocompatibility and to prevent aggregation.[35–38] Poly(ethylene glycol) (PEG) is a hydrophilic polymer commonly used to coat nanoparticles due its ability to prevent protein adsorption and aggregation.[36, 37, 39, 40] Many as-synthesized nanoparticles tend to aggregate when proteins adsorb to the surface or in media with high ionic strength, like blood plasma.[38] The silica shell provides a robust surface for PEG grafting, and PEG would likely be lost without it. A carboxy-terminated version of PEG was grafted onto bare **Hf-UiO**, but was lost, as the MOF surface is prone to corrosion/dissolution under physiological conditions. A siloxy-terminated version of PEG ($(OEt)_3Si\text{-}PEG_{2000}\text{-}OCH_3$) was synthesized and grafted onto **Hf-UiO**@SiO_2 by stirring the particles in a solution of $(OEt)_3Si\text{-}PEG_{2000}\text{-}OCH_3$ in ethanol under basic conditions (NH_4OH) to produce **Hf-UiO**@SiO_2@PEG. The PEGylated particles look similar to the silica-coated particles by TEM (Fig. 3B). TGA shows an additional weight loss step corresponding to 8.0 wt% PEG. PEG grafting raises the zeta potential closer to neutral, from −32.8 to −17.3 mV, due to the presence of a neutral polymer coating. The average size was measured by dynamic light scattering (DLS) to be 246 nm, somewhat larger than then 175 nm and 169 nm average sizes for **Hf-UiO**@SiO_2 and **Hf-UiO**, respectively. The increase in particle size upon pegylation could partially be due to slight aggregation of the **Hf-UiO**@SiO_2@PEG particles in 10 mM PBS.

In vivo CT studies

In vivo CT imaging was performed on mice using a micro-CT scanner with a carbon nanotube X-ray source, which could be synchronized and gated with physiological signals.[41, 42] Mouse respiration and electrocardiography (ECG) traces were monitored to allow respiration-gated and cardiac-gated scans that minimize image blurriness caused by the animal's motion. A 20 g anesthetized mouse was administered 6.5 mg **Hf-UiO**@SiO_2@PEG (46.4 wt% Hf, 3.0 mg Hf) via tail vein injection. In general, a change in HU of 10–15 units is considered detectable, while a change of 100 HU or more is more desirable for unambiguous diagnosis of diseased states.[4] The attenuation of the spleen and liver increased by 131 and 86 HU, respectively, while there was no attenuation enhancement in the bloodstream, as measured in the heart 15 min after injection (Fig. 4). Based on the attenuation data from the phantom studies and the sizes of the organs, about 6% of the particles accumulated in the spleen, while about 50% accumulated in the liver. This result indicates that the particles were taken up by the mononuclear phagocyte system (MPS), as the spleen and liver are rich in macrophages. This may be due to the relatively large size of **UiO**@SiO_2@PEG particles, as particles (and aggregates) larger than about 200 nm tend to be quickly filtered by the tissue in the spleen,[38] and those larger than about 500 nm tend to be taken up readily by macrophages.[43]

Small Hf-NMOF for in vivo CT

Smaller Hf-NMOF particles (**Hf-NMOF**) were made in hopes that smaller particles would circulate longer and allow blood pool imaging. **Hf-NMOF** was synthesized by heating a solution of equal molar $HfCl_4$ and H_2BDC in DMF at 100 °C in a sealed vessel for 48 h. This is the same method as used for **Hf-UiO**, but the concentration of starting materials was lowered and the acid modulator was eliminated in order to decrease the size of the particles. The resulting spherical particles were about 50 nm in diameter by SEM (Fig. 5A). TGA showed that **Hf-NMOF** has the same Hf content as **Hf-UiO** (57.3 wt%), but PXRD showed that the smaller particles are amorphous. **Hf-NMOF** was coated with silica and then PEGylated, in a manner similar to **Hf-UiO**, to result in **Hf-NMOF**@SiO_2@PEG particles that contain 9.1 wt% SiO_2, 10.8 wt% PEG, and 46.5 wt% Hf, as determined by TGA. DLS in 10 mM PBS showed an average size of 102 nm, compared to 246 nm for the corresponding larger **Hf-UiO**@SiO_2@PEG particles (Fig. S5). A test for non-specific protein adsorption was done to determine how **Hf-** NMOF@SiO_2@PEG may behave in the

bloodstream. Bovine serum albumin (BSA) was added to **Hf- NMOF**@SiO_2@PEG in a 5:1 ratio (by weight) and particle size was monitored by DLS over 95 min. Aggregation due to protein adsorption would be apparent by an increasing Z-average (an intensity-weighted measurement of particle diameter) and a decreasing signal intensity due to sedimentation of large aggregates. The Z-average stayed within a small range (192–200 nm) over the course of the experiment, and the signal intensity (counts) remained fairly constant, indicating the stability of **Hf-NMOF**@SiO_2@PEG against aggregation in the presence of BSA (Fig. 5B).

In vivo CT imaging was done using **Hf-NMOF**@SiO_2@PEG. A 20 g anesthetized mouse was administered 4.3 mg **Hf-NMOF**@SiO_2@PEG (46.5 wt% Hf, 2.0 mg Hf) via tail vein injection. As with the larger particles, these smaller particles accumulated in the spleen and liver (Fig. S6), with attenuation increases of 101 and 41 HU, respectively, and no increase in attenuation in the bloodstream. The CT results obtained using **Hf-NMOF**@SiO_2@PEG are similar to those with larger **Hf-UiO**@SiO_2@PEG. It is possible that these smaller particles still form aggregates in the bloodstream that are big enough to be filtered by spleen or easily recognized by the MPS due to ineffective PEG shielding.

Conclusions

Nanoscale metal-organic frameworks with Zr or Hf metal connecting points have been synthesized and evaluated for their potential as CT contrast agents. Both amorphous Hf-NMOF and crystalline Hf-NMOF of the UiO structure were prepared for the first time, and coated with silica and then functionalized with PEG to make the particles suitable for *in vivo* CT imaging. PEGylated Hf-NMOFs could be used as contrast agents for imaging the spleen or liver. The NMOF platform provides a promising strategy for incorporating high loadings of heavy elements into nanoparticles that can be surface-functionalized for enhanced biocompatibility and *in vivo* performance.

Supplementary Material

Refer to Web version on PubMed Central for supplementary material.

Acknowledgments

We acknowledge financial support from the NIH (U01-CA151455 and U54-151652). K.E.d. acknowledges support from the UNC Graduate School for a Dissertation Completion Fellowship. We thank Dr. Hong Yuan for help with in vivo CT imaging studies.

Notes and references

1. Seeram, E. Computed Tomography: Physical Principles, Clinical Application, and Quality Control. 3. Saunders/Elsevier; St. Louis: 2009.
2. Kalender WA. Phys Med Biol. 2006; 51:R29. [PubMed: 16790909]
3. Rutten A, Prokop M. Anti-Cancer Agents Med Chem. 2007; 7:307.
4. Speck, U. Handbook of Experimental Pharmacology. Semmler, W.; Schwaiger, M., editors. Vol. 185. Springer-Verlag; Berlin: 2008. p. 167
5. Krause, W.; Schneider, PW. Topics in Current Chemistry. Krause, W., editor. Vol. 222. Springer-Verlag; Berlin: 2002. p. 107
6. Yu S, Watson AD. Chem Rev. 1999; 99:2353. [PubMed: 11749484]
7. Matsuura N, Rowlands JA. Med Phys. 2008; 35:4474. [PubMed: 18975695]
8. Rabin O, Perez JM, Grimm J, Wojtkiewicz G, Weissleder R. Nat Mater. 2006; 5:118. [PubMed: 16444262]
9. Kim D, Park S, Lee JH, Jeong YY, Jon S. J Am Chem Soc. 2007; 129:7661. [PubMed: 17530850]

10. Kattumuri V, Katti K, Bhaskaran S, Boote EJ, Casteel SW, Fent GM, Robertson DJ, Chandrasekhar M, Kannan R, Katti KV. Small. 2007; 3:333. [PubMed: 17262759]
11. Pan D, Williams TA, Senpan A, Allen JS, Scott MJ, Gaffney PJ, Wickline SA, Lanza GM. J Am Chem Soc. 2009; 131:15522. [PubMed: 19795893]
12. Hyafil F, Cornily J-C, Feig JE, Gordon R, Vucic E, Amirbekian V, Fisher EA, Fuster V, Feldman LJ, Fayad ZA. Nat Med. 2007; 13:636. [PubMed: 17417649]
13. Galperin A, Margel D, Baniel J, Dank G, Biton H, Margel S. Biomaterials. 2007; 28:4461. [PubMed: 17644171]
14. deKrafft KE, Xie Z, Cao G, Tran S, Ma L, Zhou OZ, Lin W. Angew Chem Int Ed. 2009; 48:9901.
15. Yaghi OM, O'Keeffe M, Ockwig NW, Chae HK, Eddaoudi M, Kim J. Nature. 2003; 423:705. [PubMed: 12802325]
16. Evans OR, Lin W. Acc Chem Res. 2002; 35:511. [PubMed: 12118990]
17. Wu C, Hu A, Zhang L, Lin W. J Am Chem Soc. 2005; 127:8940. [PubMed: 15969557]
18. Férey G, Mellot-Draznieks C, Serre C, Millange F. Acc Chem Res. 2005; 38:217. [PubMed: 15835868]
19. Lin W, Rieter WJ, Taylor KML. Angew Chem Int Ed. 2009; 48:650.
20. Spokoyny AM, Kim D, Sumrein A, Mirkin CA. Chem Soc Rev. 2009; 38:1218. [PubMed: 19384433]
21. Rieter WJ, Taylor KML, Lin W. J Am Chem Soc. 2007; 129:9852. [PubMed: 17645339]
22. Rieter WJ, Taylor KML, An H, Lin W, Lin WJ. J Am Chem Soc. 2006; 128:9024. [PubMed: 16834362]
23. Taylor KML, Rieter WJ, Lin W. J Am Chem Soc. 2008; 130:14358. [PubMed: 18844356]
24. Rieter WJ, Pott KM, Taylor KML, Lin W. J Am Chem Soc. 2008; 130:11584. [PubMed: 18686947]
25. Cavka JH, Jakobsen S, Olsbye U, Guillou N, Lamberti C, Bordiga S, Lillerud KP. J Am Chem Soc. 2008; 130:13850. [PubMed: 18817383]
26. Kandiah M, Nilsen MH, Usseglio S, Jakobsen S, Olsbye U, Tilset M, Larabi C, Quadrelli EA, Bonino F, Lillerud KP. Chem Mater. 2010; 22:6632.
27. Umemura A, Diring S, Furukawa S, Uehara H, Tsuruoka T. J Am Chem Soc. 2011; 133:15506. [PubMed: 21861521]
28. Schaate A, Roy P, Godt A, Lippke J, Waltz F. Chem Eur J. 2011; 17:6643. [PubMed: 21547962]
29. Wang C, deKrafft KE, Lin W. J Am Chem Soc. 2012; 134:7211. [PubMed: 22486151]
30. Brooks RA. J Comput Assist Tomo. 1977; 1:487.
31. National Institute of Standards and Technology. [accessed Feb 5, 2012] X-ray Mass Attenuation Coefficients. http://www.physics.nist.gov/PhysRefData/XrayMassCoef/tab3.html
32. Sprawls, P. Physical Principles of Medical Imaging. Aspen Publishers; Gaithersburg, MD: 1993.
33. Huxford RC, deKrafft KE, Boyle WS, Liu D, Lin W. Chem Sci. 2012; 3:198.
34. Liu D, Huxford RC, Lin W. Angew Chem Int Ed. 2011; 50:3696.
35. Ferrari M. Nat Rev Cancer. 2005; 5:161. [PubMed: 15738981]
36. Karakoti AS, Das S, Thevuthasan S, Seal S. Angew Chem Int Ed. 2011; 50:2.
37. Harris, JM.; Zalipsky, S., editors. Poly(Ethylene Glycol): Chemistry and Biological Applications. American Chemical Society; Washington, DC: 1997.
38. Walkey CD, Chan WCW. Chem Soc Rev. 2012; 41:2780. [PubMed: 22086677]
39. Otsuka H, Nagasaki Y, Kataoka K. Adv Drug Deliv Rev. 2003; 55:403. [PubMed: 12628324]
40. Prencipe G, Tabakman SM, Welsher K, Liu Z, Goodwin AP, Zhang L, Henry J, Dai H. J Am Chem Soc. 2009; 131:4783. [PubMed: 19173646]
41. Cao G, Calderon-Colon X, Wang P, Burk L, Lee YZ, Rajaram R, Sultana S, Lalush D, Lu J, Zhou O. Proc of SPIE. 2009; 7258:72585Q1–7.
42. Cao G, Lee YZ, Peng R, Liu Z, Rajaram R, Calderon-Colon X, An L, Wang P, Phan T, Sultana S, Lalush DS, Lu JP, Zhou O. Phys Med Biol. 2009; 54:2323. [PubMed: 19321922]

43. Mansour HM, Rhee Y-S, Wu X. Int J Nanomed. 2009; 4:299. Hf-based nanoscale metal-organic frameworks were coated with silica and poly(ethylene glycol), and used as contrast agents for computed tomography imaging.

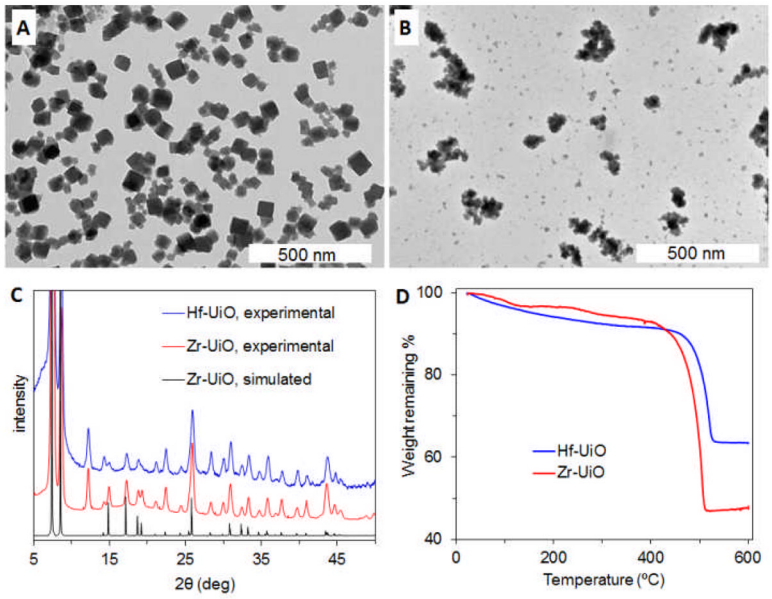

Fig. 1.

TEM images of (A) **Zr-UiO** and (B) **Hf-UiO**. (C) Experimental PXRD patterns of **Zr-UiO** and **Hf-UiO**, along with the simulated pattern for **Zr-UiO**. (D) TGA curves of **Zr-UiO** and **Hf-UiO**.

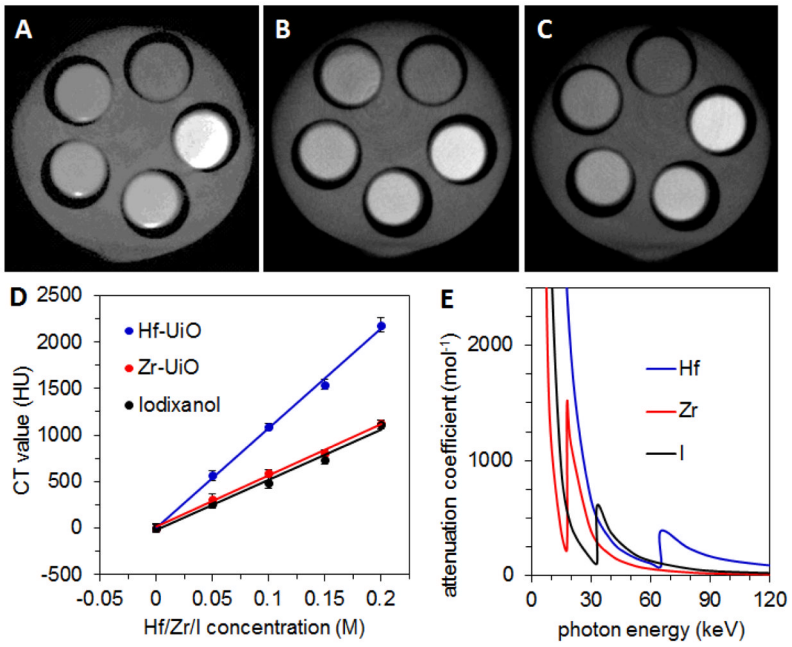

Fig. 2.

CT phantom images of (A) **Hf-UiO**, (B) **Zr-UiO**, and (C) Iodixanol dispersed in water. From the top, counterclockwise, the slots have [Hf/Zr/I] = 0, 0.05, 0.10, 0.15, and 0.20 M. (D) X-ray attenuation as a function of [Hf/Zr/I] for **Hf-UiO**, **Zr-UiO**, and **Iodixanol** at 50 kVp. (E) Attenuation coefficient vs. photon energy for Hf, Zr, and I.

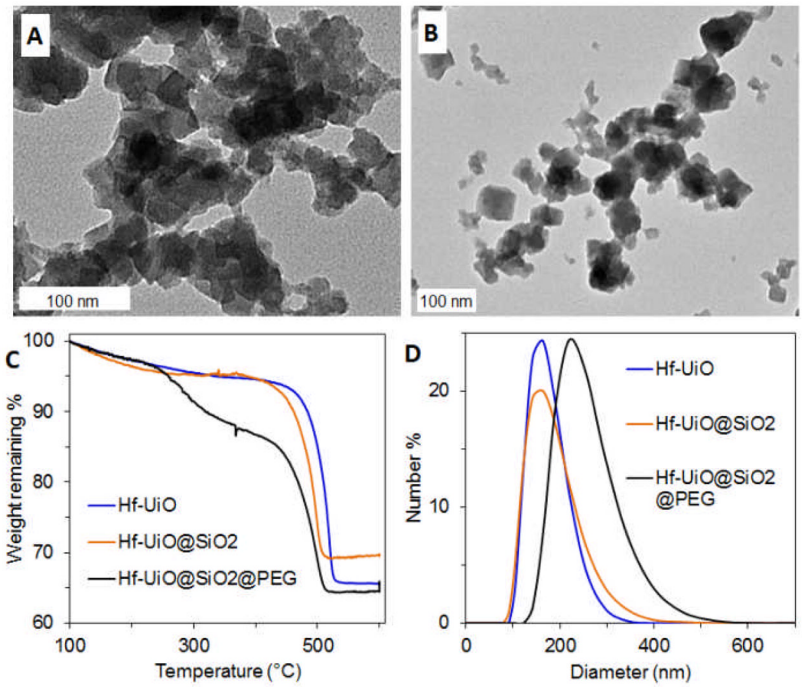

Fig. 3.

TEM images of (A) **Hf-UiO**@SiO_2 and (B) **Hf-UiO**@SiO_2@PEG. (C) TGA of **Hf-UiO**, **Hf-UiO**@SiO_2, and **Hf-UiO**@SiO_2@PEG. (D) Size distribution by number obtained by DLS of Hf-UiO, **Hf-UiO**@SiO_2, and **Hf-UiO**@SiO_2@PEG in 10 mM PBS.

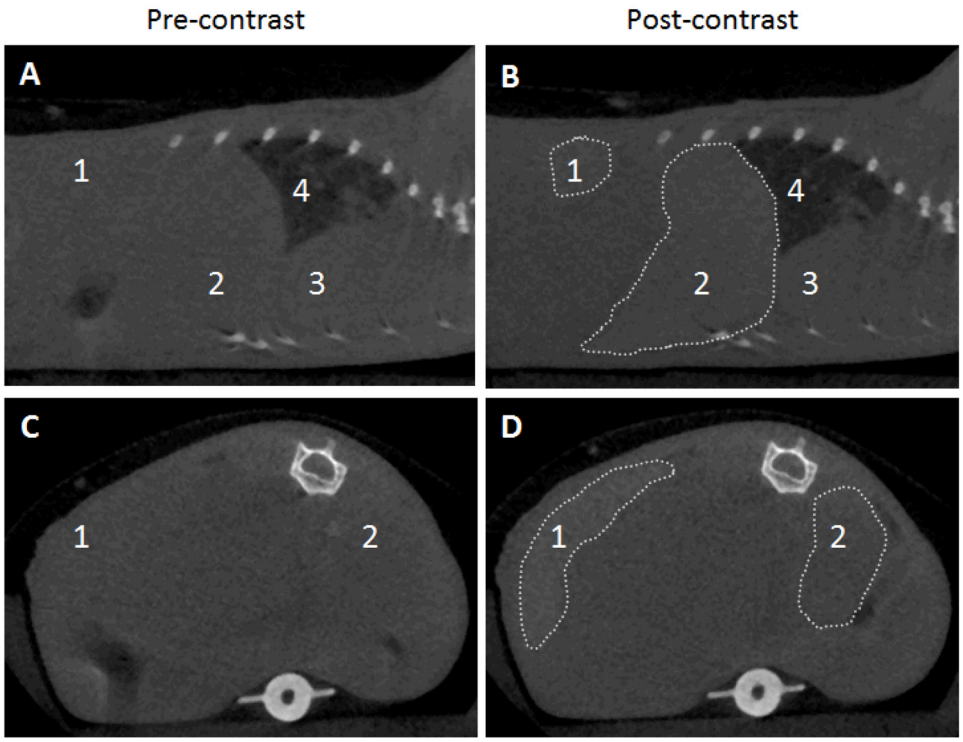

Fig. 4.

(A,B) Sagittal and (C,D) axial CT slices of a mouse pre-contrast and 15 min after injection of **Hf-UiO**@SiO_2@PEG. The areas of increased attenuation are outlined, and the labels are: 1-spleen (+131 HU), 2-liver (+86 HU), 3-heart, 4-lungs.

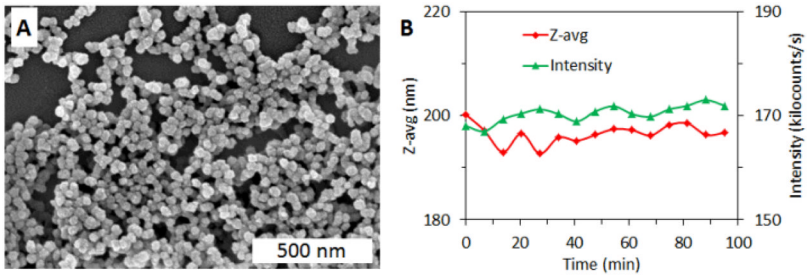

Fig. 5.

(A) SEM image of **Hf-NMOF**@SiO_2@PEG. (B) DLS stability test of **Hf-NMOF**@SiO_2@PEG in 10 mM PBS in the presence of bovine serum albumin.

Table 1

Hf-UiO and its modifications: weight %, zeta potential, and size.

	Weight %[a]				
Sample	**Hf**	**SiO_2**	**PEG**	**Zeta potential (mV)[b]**	**Average size (nm)[c]**
Hf-UiO	57.3	-	-	−24.6	169
Hf-UiO@SiO_2	50.4	13.2	-	−32.8	175
Hf-UiO@SiO_2@PEG	46.4	12.2	8.0	−17.3	246

[a] Determined by TGA.

[b] Measured in 1 mM aq. KCl.

[c] Number-averaged sizes measured in 10 mM PBS.